Full field model for interleave-chirped arrayed waveguide gratings

Bernardo Gargallo[1,⋆] **and Pascual Muñoz**[1,2]

[1]*Optical and Quantum Communications Group, iTEAM - Universitat Politècnica de València C/ Camino de Vera s/n - Valencia 46022 - SPAIN*
[2]*VLC Photonics S.L., C/ Camino de Vera s/n - Valencia 46022 - SPAIN*
[⋆]*bergarja@iteam.upv.es*

Abstract: In this paper, a theoretical model for an Interleave-Chirped Arrayed Waveguide Grating (IC-AWG) is presented. The model describes the operation of the device by means of a field (amplitude and phase) transfer response. The validation of the model is accomplished by means of simulations, using parameters from previously fabricated devices. A novel design procedure is derived from the model, and it is later on employed to demonstrate the design of colorless universal IC-AWGs. The model can be readily applied to the analysis and design of future multi-wavelength optical coherent communications receivers and optical waveform analyzers.

OCIS codes: (060.1660) Coherent optical communications; (070.2580) Paraxial wave optics; (130.3120) Integrated optics devices; (130.5440) Polarization-selective devices; (130.7408) Wavelength filtering devices.

References and links

1. K. Kikuchi, "Coherent optical communications: historical perspectives and future directions," in *High Spectral Density Optical Communication Technology*, M. Nakazawa, K. Kikuchi, and T. Miyazaki, eds (Springer, 2010), Chap. 2.
2. R. Nagarajan e.a., "Terabit/s class InP photonic integrated circuits," Semicond. Sci. Tech. **27**, 094003 (2012).
3. J. T. Rahn e.a., "250 Gb/s real-time PIC-based super-channel transmission over a gridless 6000 km terrestrial link," in Proc. Opt. Fiber Comm. conference paper PDP5D.5 (2012).
4. L. B. Soldano and E. C. M. Pennings, "Optical multi-mode interference devices based on self-imaging: principles and applications," J. Lightwave Technol. **4**, 615–627 (1995).
5. M. Bachmann, P. Besse, and H. Melchior, "General self-imaging properties in N x N multimode interference couplers including phase relations," Appl. Opt. **33**, 3905–3911 (1994).
6. J. M. Heaton and R. M. Jenkins, "General matrix theory of self-imaging in multimode interference (MMI) couplers," IEEE Photonic Tech. L. **11**, 212–214 (1999).
7. J. Van Roey, J. van der Donk, and P. Lagasse, "Beam-propagation method: analysis and assessment," J. Opt. Soc. Am. **71**, 803-810 (1981).
8. C. R. Doerr, L. Zhang, and P. J. Winzer, "Monolithic InP multiwavelength coherent receiver using a chirped arrayed waveguide grating," J. Lightwave Technol. **29**, 536–541 (2011).
9. P. Muñoz, D. Pastor, and J. Capmany, "Modeling and design of arrayed waveguide gratings," J. Lightwave Technol. **20**, 661–674 (2002).
10. H. Takahashi, K. Oda, H. Toba, and Y. Inoue, "Transmission characteristics of arrayed waveguide N x N wavelength multiplexer," J. Lightwave Technol. **13**, 447–455 (1995).
11. Y. Wan and R. Hui, "Design of WDM cross connect based on interleaved AWG (IAWG) and a phase shifter array," J. Lightwave Technol. **25**, 1390–1400 (2007).
12. J. W. Goodman, "Introduction to Fourier optics," in *Classic Textbook Reissue Series*, W. Stephen, ed. (New York: McGraw-Hill, 1988), ch. 5, pp. 83–90.
13. L. H. Spiekman, M. R. Amersfoort, A. H. de Vreede, F. P. G. M. van Ham, A. Kuntze, J. W. Pedersen, P. Demeester, and M. K. Smit, "Design and realization of polarization independent phased array wavelength demultiplexers using different array orders for TE and TM," J. Lightwave Technol. **14**, 991–995 (1996).

14. C. R. Doerr, L. Zhang, L. Buhl, V. I. Kopp, D. Neugroschl, and G. Weiner, "Tapered dual-core fiber for efficient and robust coupling to InP photonic integrated circuits," Proc. OFC paper OThN5 (2009).
15. M. Lohmeyer, "Wave-matching-method for mode analysis of dielectric waveguides," Opt. Quant. Electron. **29**, 907–922 (1997).
16. FieldDesigner™, PhoeniX Software, http://www.phoenixbv.com.
17. M. K. Smit and C. van Dam, "PHASAR-based WDM-devices: Principles, design and applications," IEEE J. Sel. Top. Quant. **2**, 236–250 (1996).
18. N. K. Fontaine, R. P. Scott, L. Zhou, F. M. Soares, J. P. Heritage, and S. J. B. Yoo, "Real-time full-field arbitrary optical waveform measurement," Nat. Photonics **4**, 248–254 (2010).
19. S. T. S. Cheung, B. Guan, S. S. Djordjevic, K. Okamoto, and S. J. B. Yoo, "Low-loss and high contrast Silicon-on-Insulator (SOI) arrayed waveguide grating," in *CLEO: Science and Innovations*, OSA Technical Digest (online) (Optical Society of America, 2012), paper CM4A.5.
20. P. Bernasconi, C. Doerr, C. Dragone, M. Cappuzzo, E. Laskowski, and A. Paunescu, "Large NxN waveguide grating routers," J. Lightwave Technol. **18**, 985–991 (2000).

1. Introduction

Coherent optical communications have revived in the recent years, due to the availability of high-speed digital electronic processors [1]. Together with high performance photonic integrated cirtuis (PICs), real-time coherent communications operating at aggregate speeds of up to 500 Gb/s have been demonstrated [2, 3]. Within the toolset for the production of integrated coherent receivers, a very relevant part is the analysis and design models, together with numerical tools. Currently, the core of integrated optics based coherent receivers are Multi-Mode Interference (MMI) couplers, designed to operate as 90° hybrids. The MMI theory is very well known, and extensive models exist to calculate the field transfer functions of such devices [4–6]. Moreover, numerical tools can be readily employed to optimize the performance of such devices, as Beam Propagation Method (BPM) in combination of Effective Index Method (EIM) [7]. The rectangular structure and paraxial nature of the MMIs result in modest computation times for those algorithms/tools, using commodity personal computers.

Similar to conventional Intensity Modulated Direct Detection (IM-DD) systems, Wavelength Division Multiplexing (WDM) has been recently brought into PICs for coherent optical communications. The natural combination of on chip demultiplexers, as the Arrayed Waveguide Grating, and optical MMI 90° hybrids have been demonstrated in [2], whereas off-chip optical polarization splitters are used to feed the PIC. Nonetheless, the solution proposed by Doerr e.a. [8] in which the AWG arms are modified to enable three fold operation (demultiplexer, polarization splitter, 90° hybrid), is envisaged as the most compact solution for these future on-chip architectures. This device is named Interleave-Chirped AWG (IC-AWG). Although in [8] an experimental demonstration of the device is given, a model for the analysis and design of the IC-AWG does not exist in the literature. The purpose of this paper is to report the development of the optical field model for the analysis and design of IC-AWGs. The paper is structured as follows. In Section 2, the theoretical equations describing the full field (amplitude and phase) transfer function for an IC-AWG are developed, taking as base our work in [9]. The model is validated in Section 3 using as IC-AWG construction parameters those of the fabricated device reported in [8]. In Section 4, a design procedure for the IC-AWG is proposed, in which the aim is to maximize the spectral usage for the wavelength channels and polarizations. The design procedure is used in Section 5 to demonstrate a colorless universal IC-AWG. Finally the outlook and conclusions are given in Section 6.

2. Theoretical model

2.1. AWG layout

A schematic design of a 2 x N Arrayed Waveguide Grating (AWG) is shown in Fig. 1(a). It consists of two input waveguides, followed by a free propagation region (FPR). At the end of this

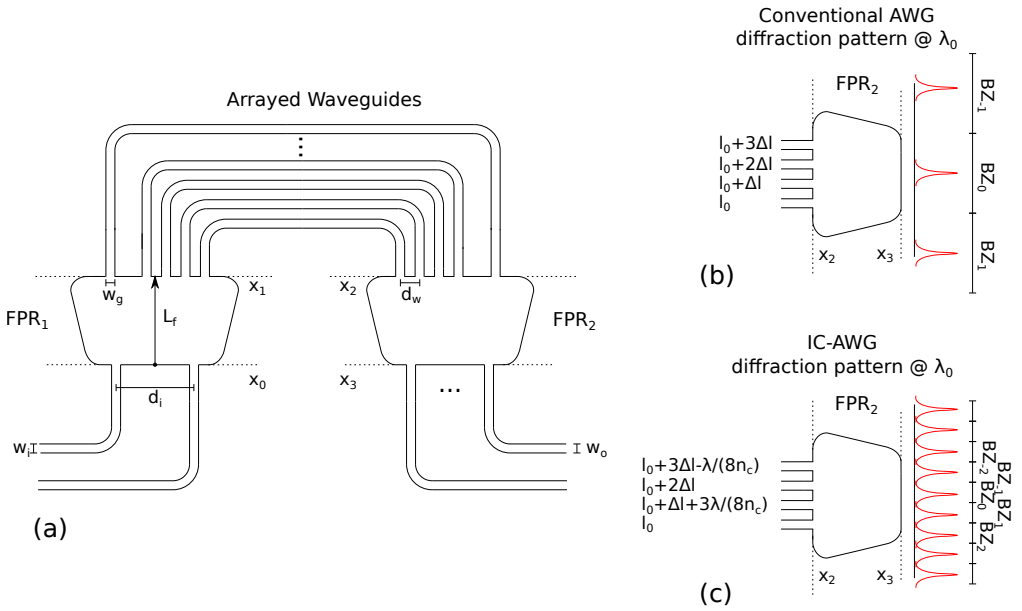

Fig. 1: (a) IC-AWG layout. (b) Field focusing points without and (c) with chirp. Abbreviations: subscripts *i*, *w* and *o* stand for input, arrayed and output waveguides, respectively; ω: waveguide width; d: waveguide spacing; L_f: focal length; FPR: free propagation region; l_0: shortest AW length; Δl: incremental length; λ: wavelength; n_c: AW effective index; BZ: Brillouin Zone.

FPR, the field is coupled in the arrayed waveguides. In a conventional AWG design, the length of a consecutive waveguides in the array differ by a constant value, Δl, which is an integer (m) multiple of the design wavelength (λ_0) within the waveguide, as shown in Fig. 1(b). The accumulated phase shift depends on wavelength/frequency, which combined with the second FPR, leads to light focusing at different output positions for each wavelength. Moreover, the field discretization imposed in the arms, causes diffraction in different orders (...,m-1,m,m+1,...), resulting in different Brillouin Zones (BZs) [10]. In an Interleave-Chirped AWG (IC-AWG), the array is divided in M subsets. Within each subset, whose waveguides are spaced Md_ω at x_1 and x_2, an additional floor length (related to λ_0) is introduced [11]. The division of the array in M subsets reduces the original BZ size by a factor M, as will be formulated in detail in the following sections. Besides, introducing different floor length in each subset, results in out of phase interference at x_3, for the fields diffracted by each subset. This can be seen in Fig. 1(c), where the width of the focusing zones has been reduced by a factor M compared to Fig. 1(b). Each group of this arrayed waveguides with the same incremental length is called subarray. Hence, if for example a $M = 4$ chirp pattern is used, the first subarray will be composed of the arrayed waveguides number $\{1,5,9,...,N\text{-}3\}$, the second by $\{2,6,10,...,N\text{-}2\}$ ... In this section, the model of the IC-AWG extending the Fourier optics AWG model presented in [9] is formulated. Table 1 shows a summary of the variables used in the formulation.

2.2. Field at the input waveguide

The field in an input waveguide placed at the middle of the first FPR, can be approximated by a power normalized Gaussian function

Table 1: Summary of the variables used in the formulation. Subscripts *i*, *g* and *o* stand for input, arrayed and output waveguides, respectively.

b_i, b_g, b_o	Power normalized Gaussian function	M	Number of sub-arrays
B_i, B_g, B_o	Spatial Fourier transform of b_x	$x_0 - x_3$	AWG planes
$\omega_i, \omega_g, \omega_o$	Mode field radius	d_i, d_w, d_o	Waveguide separation
γ	Frequency spatial dispersion parameter	L_f	Focal length
α	Wavelength focal length in Fourier optics	ν	Frequency
n_s	Slab effective index	n_g	Group index
n_c	Array waveguides effective index	N	Number of array waveguides
r	Waveguide number in the array waveguides	m	Grating order
$l_{r,k}$	Length of the r waveguide in subarray k	β	Propagation constant
$l_{c,k}$	Length of the shortest waveguide in subarray k	c	Speed of light in vacuum
Δl	Incremental length between AWs	λ	Wavelength
$\Delta l'$	Incremental length between AWs in a subarray	L_u	Loss nonuniformity
Δf_{ch}	Separation between channels in frequency	$f_1 - f_3$	Total field distributions
t	Field at the output waveguides	q	Number of the output waveguide
$\Delta\nu_{pol}$	Frequency separation between polarizations	$\Delta\nu_{bw}$	Frequency 3-dB bandwidth
Δx_{pol}	Spatial separation between polarizations	Δx_{FSR}	Spatial FSR

$$b_i(x_0) = \sqrt[4]{\frac{2}{\pi\omega_i^2}} e^{-\left(\frac{x_0}{\omega_i}\right)^2} \tag{1}$$

where ω_i is the mode field radius and x_0 is the spatial coordinate at the input plane, as is shown in Fig. 1(a). Although the Gaussian approximation is suitable to clarify the understanding of the device and enables to obtain a final analytical expression, it fails in predicting the response outside the band, thus is necessary the use of real modes to obtain simulation responses closer to the real physical response, as detailed in [9].

2.3. First Free Propagation Region

This field is radiated to the first FPR, and the light spatial distribution can be obtained by the spatial Fourier transform of the input distribution, using the paraxial approximation [9, 12]:

$$B_i(x_1) = \mathscr{F}\{b_i(x_0)\}|_{u=\frac{x_1}{\alpha}} = \sqrt[4]{2\pi\frac{\omega_i^2}{\alpha^2}} e^{-\left(\pi\omega_i\left(\frac{x_1}{\alpha}\right)\right)^2} \tag{2}$$

where u is the spatial frequency domain variable of the Fourier transform and α is the equivalent to the wavelength focal length product in Fourier optics propagation [12], expressed as:

$$\alpha = \frac{cL_f}{n_s\nu} \tag{3}$$

being L_f the slab length, n_s the effective index of the FPR, ν the frequency and c the speed of light in vacuum. The paraxial approximation holds in the Fraunhofer diffraction region, which corresponds to the AWG slab lengths accomplishing $L_f \gg \left(\pi W_x^2\right)/(4\lambda)$ [12]. For typical waveguide widths $W_x = 1.5\ \mu$m and wavelength value $\lambda = 1550$ nm, this approximation is valid for $L_f \gg 1.14\ \mu$m. The total field distribution for an arbitrary number of illuminated arrayed waveguides (AWs), placed at the x_1 plane, is:

$$f_1(x_1) = \sqrt[4]{2\pi\omega_g^2} \sum_{k=0}^{M-1} \left[\sum_r B_i(Mrd_\omega + kd_\omega)\, b_g(x_1 - Mrd_\omega - kd_\omega) \right] \tag{4}$$

where d_ω is the spacing between arrayed waveguides, Fig. 1(a), r is the AW number and ω_g is the mode field radius of the arrayed waveguide, M is the length of the chirp pattern (and

the number of waveguide array subsets) and $b_g(x)$ is the Gaussian approximation as in Eq. (1) for the field in the AW. Particularizing for a set of an arbitrary number N of illuminated waveguides:

$$f_1(x_1) = \sqrt[4]{2\pi\omega_g^2}\sum_{k=0}^{M-1}\left[\prod\left(\frac{x_1}{Nd_\omega}\right)B_i(x_1)\sum_{r=-\infty}^{+\infty}\delta(x_1 - Mrd_\omega - kd_\omega)\right]\otimes b_g(x_1) \tag{5}$$

with $\otimes$ being the convolution, and $\prod(x_1/Nd_\omega)$ being a truncation function defined as:

$$\prod\left(\frac{x_1}{Nd_\omega}\right) = \begin{cases} 1, & \text{if } |x| \leq \frac{Nd_\omega}{2} \\ 0, & \text{otherwise} \end{cases} \tag{6}$$

2.4. Field at the arrayed waveguides

Let the length of waveguide number r in each subarray be given by,

$$l_{r,k} = l_{c,k} + \Delta l'\left(r + \frac{N}{2M}\right) \tag{7}$$

with $\Delta l'$ being the incremental length between one waveguide and the next in the same subarray, and $l_{c,k}$ being the length of the shortest waveguide in subarray number k, used to account for different floor length in each subarray and to introduce the chirp pattern in the AWs. The conventional AWG has a path length increment

$$\Delta l = \frac{m\lambda_0}{n_c} \tag{8}$$

In this equation, m is the grating order, n_c is the effective index in the waveguides and λ_0 is the design central wavelength. In order to keep similar focusing properties for all the M subarrays, $\Delta l' = M\Delta l$. The phase shift introduced by waveguide r can be expressed as

$$\phi_{r,k}(\nu) = e^{-j\beta l_{r,k}} = e^{-j\beta\left(l_{c,k} + \Delta l'\left(r + \frac{N}{2M}\right)\right)} \tag{9}$$

being β the propagation constant for the AW:

$$\beta = \frac{2\pi n_c \nu}{c} \tag{10}$$

Using Eqs. (5) and (9) the field distribution at x_2 is given by:

$$f_2(x_2,\nu) = \sqrt[4]{2\pi\omega_g^2}\sum_{k=0}^{M-1}\left\{\prod\left(\frac{x_2}{Nd_\omega}\right)B_i(x_2)\,\phi_k(x_2,\nu)\,\delta_{\omega,k}(x_2)\,e^{j\beta\Delta l'\frac{k}{M}}\right\}\otimes b_g(x_2) \tag{11}$$

with

$$\delta_{\omega,k}(x_2) = \sum_{r=-\infty}^{+\infty}\delta(x_2 - Mrd_\omega - kd_\omega) \tag{12}$$

$$\phi_k(x_2,\nu) = \psi_k(\nu)\,e^{-j\beta\Delta l'\frac{x_2}{Md_\omega}} \tag{13}$$

$$\psi_k(\nu) = e^{-j\beta\left(l_{c,k} + \Delta l'\frac{N}{2M}\right)} \tag{14}$$

2.5. Second Free Propagation Region

To obtain the spatial field distribution at the end of the second FPR, the spatial Fourier transform of equation (11) is calculated as follows:

$$f_3(x_3,\nu) = \sqrt[4]{2\pi\omega_g^2}B_g(x_3)\sum_{k=0}^{M-1}\left[\operatorname{sinc}\left(Nd_\omega\frac{x_3}{\alpha}\right)\otimes b_i(x_3)\otimes\Phi_k(x_3,\nu)\otimes\Delta_{\omega,k}(x_3)\,e^{j\beta\Delta l'\frac{k}{M}}\right] \tag{15}$$

with,

$$\Phi_k(x_3,\nu) = \mathscr{F}\left\{\psi_k(\nu)\,e^{-j\beta\Delta l'\frac{x_2}{Md_\omega}}\right\}\Big|_{u=\frac{x_3}{\alpha}} = \psi_k(\nu)\,\delta\left(x_3+\frac{n_c\nu\Delta l'\alpha}{cMd_\omega}\right) \tag{16}$$

$$\Delta_{\omega,k}(x_3) = \mathscr{F}\left\{\sum_{r=-\infty}^{+\infty}\delta(x_2-Mrd_\omega-kd_\omega)\right\}\Big|_{u=\frac{x_3}{\alpha}} = \frac{1}{M}\sum_{r=-\infty}^{+\infty}e^{-j2\pi kd_\omega\frac{x_3}{\alpha}}\,\delta\left(x_3-r\frac{\alpha}{Md_\omega}\right) \tag{17}$$

which after some manipulation results in:

$$f_3(x_3,\nu) = \sqrt[4]{2\pi\frac{\omega_g^2}{\alpha^2}}B_g(x_3)\,\frac{1}{M}\sum_{k=0}^{M-1}\left[\psi_k(\nu)\,e^{j\beta\Delta l'\frac{k}{M}}\sum_{r=-\infty}^{+\infty}e^{-j2\pi r\frac{k}{M}}\,f_M\left(x_3-r\frac{\alpha}{Md_\omega}+\frac{n_c\nu\Delta l'\alpha}{cMd_\omega}\right)\right] \tag{18}$$

with,

$$f_M(x_3) = \operatorname{sinc}\left(Nd_\omega\frac{x_3}{\alpha}\right)\otimes b_i(x_3) \tag{19}$$

The argument of f_M in Eq. (18) shows the field at the output of the second FPR has its focusing point position determined by the number of subarrays, M, and the incremental length, $\Delta l'$. Moreover, the term $e^{j\beta\Delta l'\frac{k}{M}}$, is a phase shift dependent of the subarray number, and the term $e^{-j2\pi r\frac{k}{M}}$ is a phase shift dependent of the focusing position. Position x_3 and wavelength $\lambda = c/\nu$ are related through the frequency spatial dispersion parameter (FSDP) given by:

$$\gamma = \frac{cMd_\omega}{n_c\Delta l'\alpha} = \frac{\nu_0 d_\omega}{\alpha m} \tag{20}$$

2.6. Field at the output waveguides

At the output waveguides, the field can be obtained through the following overlap integral:

$$t_{0,q}(\nu) = \int_{-\infty}^{+\infty} f_3(x_3,\nu)\,b_0(x_3-qd_0)\,\partial x_3 \tag{21}$$

where b_0 is the fundamental mode profile at the output waveguide (OW), q is the OW number and d_0 is the OW spacing.

2.7. Arbitrary IW position

All this formulation can be easily extended to the case with more than one input waveguide (IW), not only for the case with one input placed at the central position of the first FPR. The field at the IW can be expressed then as

$$b_{i,p}(x_0) = \sqrt[4]{\frac{2}{\pi\omega_i^2}} e^{-\left(\frac{x_0 - pd_i}{\omega_i}\right)^2} = b_{i,p}(x_0 - pd_i) \tag{22}$$

where p is the IW number and d_i is the IW spacing. At the output plane the field will be

$$f_3(x_3, \nu) = \sqrt[4]{2\pi\frac{\omega_g^2}{\alpha^2}} B_g(x_3) \frac{1}{M} \sum_{k=0}^{M-1} \left[\psi_k(\nu) e^{j\beta\Delta l' \frac{k}{M}} \sum_{r=-\infty}^{+\infty} e^{-j2\pi r \frac{k}{M}} f_M\left(x_3 - r\frac{\alpha}{Md_\omega} + \frac{n_c \nu \Delta l' \alpha}{cMd_\omega} + pd_i\right) \right] \tag{23}$$

and the field in the output waveguides is

$$t_{p,q}(\nu) = \int_{-\infty}^{+\infty} f_{3,p}(x_3, \nu)\, b_0(x_3 - qd_0)\, \partial x_3 \tag{24}$$

2.8. Modeling polarization dependence

This model can also be extended to the case where two polarizations are supported by the waveguiding structures. Although polarization dependence is minimized in conventional AWG [13], it can be exploited in emerging applications, as discussed in the introduction. Through Eq. (23) the shift between polarizations is given by:

$$\Delta x_{pol} = \frac{m}{d_\omega}\left(\alpha_{TM}(\nu) - \frac{n_{c,TM}(\nu)\,\alpha_{TM}(\nu)\,\nu}{n_{c,TE}(\nu_0)\,\nu_0} - \alpha_{TE}(\nu) + \frac{n_{c,TE}(\nu)\,\alpha_{TE}(\nu)\,\nu}{n_{c,TE}(\nu_0)\,\nu_0}\right) \tag{25}$$

The equation indicates that at the output plane each polarization is going to be focused at different position. The distance between TE and TM polarization focusing points, at a given ν, depends on the spacing, length and effective index of the AWs and length of the FPR. The frequency shift corresponding to the aforementioned distances, which in the literature is known as Polarization Dependent Wavelength Shift (PDWS) [13], is given by:

$$\begin{aligned}\Delta\nu_{pol} = \frac{n_{c,TE}(\nu_o)\,\nu_o}{n_{c,TM}(\nu + \Delta\nu_{pol})} - \nu - \frac{\alpha_{TE}(\nu)\,n_{c,TE}(\nu_o)\,\nu_o}{n_{c,TM}(\nu + \Delta\nu_{pol})\,\alpha_{TM}(\nu + \Delta\nu_{pol})} \\ + \frac{\alpha_{TE}(\nu)\,n_{c,TE}(\nu)\,\nu}{n_{c,TM}(\nu + \Delta\nu_{pol})\,\alpha_{TM}(\nu + \Delta\nu_{pol})}\end{aligned} \tag{26}$$

Equation (26) shows the wavelength separation between both polarizations as a function of the effective index of the AWs and the FPRs length. For $\nu = \nu_0$ it reduces to:

$$\Delta\nu_{pol} = \frac{n_{c,TE}(\nu_0)\,\nu_0}{n_{c,TM}(\nu_0 + \Delta\nu_{pol})} - \nu_0 \tag{27}$$

Equation (27) is extremely important in the design of the IC-AWG, since it shows that the PDWS only depends on the effective index of each polarization, and ν_0. For the design of IC-AWGs, described in Section 4, it will restrict the number of channels and their frequency spacing.

3. Simulation of a fabricated and reported device

In this section, the model is particularized to the case of the device reported in [8]. In [8], it is mentioned that it is possible to find a $M = 4$ chirp pattern that produces four

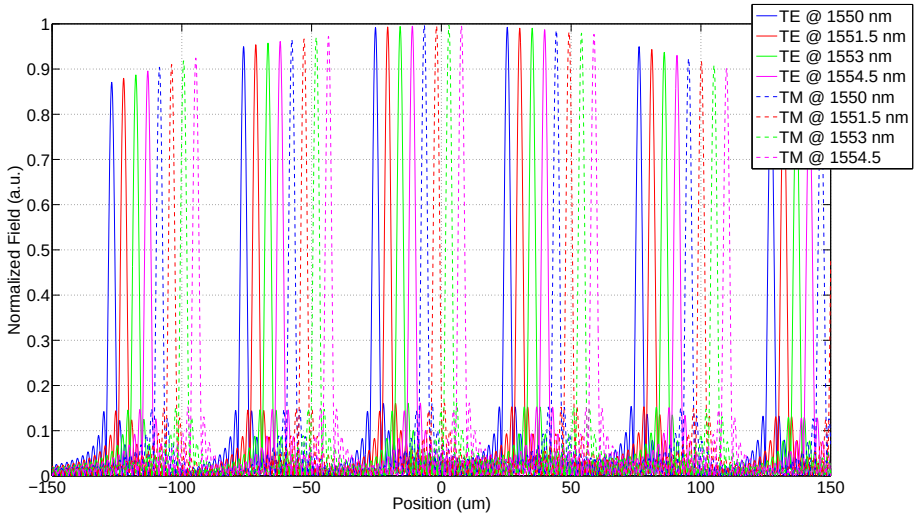

Fig. 2: $f_3(x_3,\lambda)$ using input waveguide 1 for each wavelength channel and polarization.

equal-power outputs with the relations of a 90° optical hybrid, being this chirp pattern $[0,3\lambda_0/(8n_c),0,-\lambda_0/(8n_c)]$, where λ_0 is the design central wavelength and n_c the effective index of the AWs. This chirp pattern can be easily introduced in the AWs through the $l_{c,k}$ parameter in Eq. (7), i.e. $l_{c,0}=0$, $l_{c,1}=3\lambda_0/(8n_c)$, $l_{c,2}=0$ and $l_{c,3}=-\lambda_0/(8n_c)$. The 90° hybrid operation consists in taking two input ligthwaves with complex amplitudes a and b, and obtaining at the output four signals of the form $(a+b)/2$, $(a+jb)/2$, $(a-b)/2$ and $(a-jb)/2$. The AWs are InP ridge waveguides, with a InGaAsP core 160 nm thick and a bandgap of 1.4 μm. The waveguide width is 2.45 μm, with an etching of 0.2 μm and a cladding height of 1 μm [14]. The effective indexes for the waveguide and FPR cross-section were calculated, both for TE and TM, using a film-mode matching (FMM) [15] commercial software [16]. Using equation (27), is possible to calculate the PDWS for these waveguides, obtaining 5.9 nm. In [8], four channels with a 185 GHz spacing are used. The IC-AWG has 100 arms, and FPR lengths of 2 mm. The AW and OW spacing is estimated to be 4.74 μm. The OW number is 32 and the grating order is $m=21$. Consequently, the incremental length between arrayed waveguides Δl in each subarray is 40.69 μm. To produce four equal-power outputs with the relations of a 90° optical hybrid, the chirp pattern used is $[0,3\lambda_0/(8n_c),0,-\lambda_0/(8n_c)]$ [11]. The width of the BZs is 1/4 of the BZs of the AWG without chirp. Placing two input waveguides, spaced by 1/4 of the BZ, i.e. with $\pi/2$ phase shift between them (the full BZ FSR corresponds to 2π), enables the operation as 90° hybrid. Hence, the two input waveguides are placed in the positions $d_{i,1}=25.4$ μm and $d_{i,2}=$ -25.4 μm.

Equations (23) and (24) are used to calculate the normalized field at the output plane x_3 for each channel and both polarizations for the input waveguide placed at the position $d_{i,1}$ (Fig. 2). The other input, placed at the position $d_{i,2}$, has identical response. Figure 2 shows how TE and TM, for a given λ, are focused at different points. Between them, a given number of additional channels can be placed, limited by the PDWS.

In Figs. 3(a) and 3(b) the transfer function at output waveguides 1 to 8 for each polarization is shown. As can be seen, the first 4 output waveguides have a maximum in the response for TE polarization at the wavelengths of the chosen channels, and the second group of 4 output

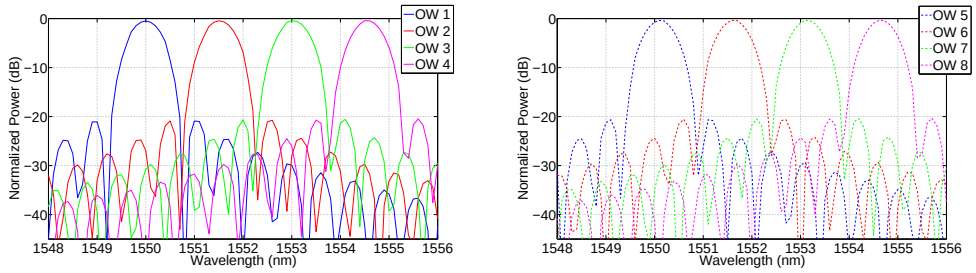

(a) $q = \{1,2,3,4\}_{TE}$ (b) $q = \{5,6,7,8\}_{TM}$

Fig. 3: Transfer function $t_{p,q}(\lambda)$ for input waveguide $p = 1$ at (a) output waveguides 1 to 4 at TE polarization and (b) output waveguides 5 to 8 at TM polarization.

waveguides have a maximum for TM polarization at the same channels. This response is repeated for the four groups of 8 output waveguides. In other words, the output waveguides 1, 9, 17 and 25 have a maximum in the response at 1550 nm and TE polarization. The same holds for TM polarization and waveguides 5, 13, 21 and 29. Then, the output waveguides 2, 10, 18 and 26 have a maximum at 1551.5 nm for TE polarization. This is repeated for each group of 4 output waveguides, so at the end there are four output waveguides for each channel and polarization. These four waveguides have the relations of a 90° optical hybrid as is shown in Figs. 4 and 5. In Fig. 4 the power and phase from the two AWG inputs (p=0,1) are plotted for each of the four output waveguides 1, 9, 17 and 25 from Fig. 4(a)-4(d) respectively. In the figures, the in-band phase response differences have been labeled. The corresponding vectorial plot at the channel center wavelength (1550 nm) and TE polarization is given in Fig. 5. As can be seen, in the 1st output waveguide the phase shift between the field in the two inputs is 135° at 1550 nm and TE polarization. At the outputs 9, 17 and 25, these phase shifts at the same wavelength and polarization are 45°, -45° and -135°, respectively.

Table 2: Number of the output waveguide for each phase shift, channel and polarization

		Channel			
Phase shift		λ_1	λ_2	λ_3	λ_4
$\Delta\phi_{in_1-in_2}$ TE	135°	1	2	3	4
	45°	9	10	11	12
	-45°	17	18	19	20
	-135°	25	26	27	28
$\Delta\phi_{in_1-in_2}$ TM	135°	5	6	7	8
	45°	13	14	15	16
	-45°	21	22	23	24
	-135°	29	30	31	32

In Table 2 a summary of the phase relations between the two inputs for each output waveguide is given. As can be seen, each group of 4 output waveguides have the necessary hybrid relations, and it is accomplished for each channel and polarization.

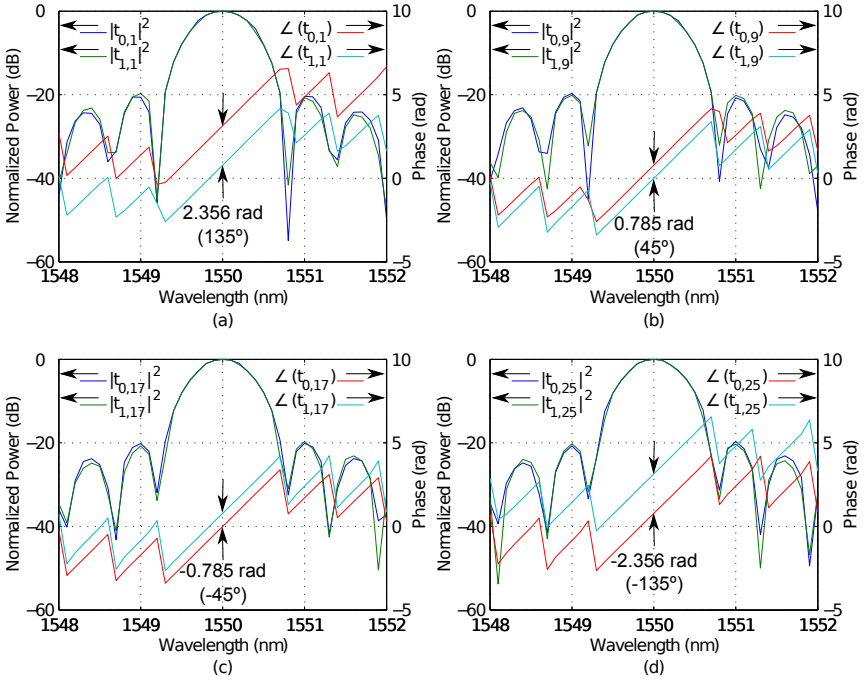

Fig. 4: Power and phase transfer functions $t_{p,q}(\lambda)$ for input waveguides $p = 0,1$ and output waveguides (a) 1, (b) 9, (c) 17 and (d) 25 for TE polarization.

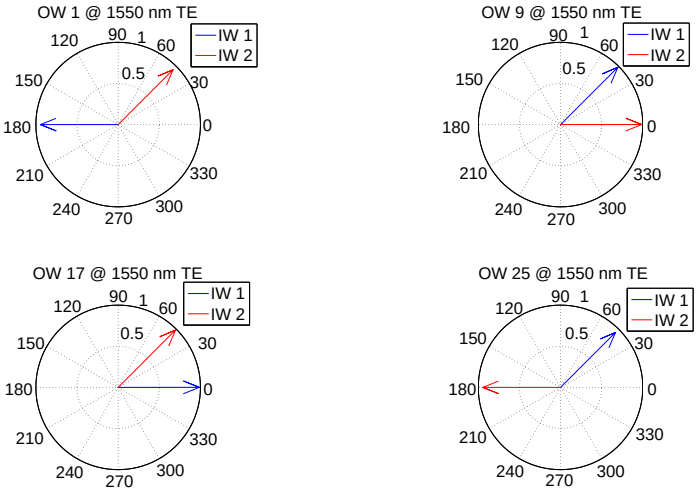

Fig. 5: Vectorial representation of the field at the output waveguides

4. Design procedure

The validation of the model presented in the previous section shows it can describe the full-field response of the IC-AWG. However, the literature lacks of a design procedure for such a special device. Using the equations derived in Section 2, is possible to obtain a design procedure for the IC-AWG. Once the design frequency ν_0 is selected, the following steps are used to obtain the physical parameters of the IC-AWG.

1. Select the number of channels and the separation between them, Δf_{ch}. This will fix the necessary polarization spacing $\Delta\nu_{pol}$ in Eq. (27), and then the geometry of the arrayed waveguides necessary to obtain the quotient between polarization effective indexes.

2. Set the spatial separation between polarizations in Eq. (25) as half free spectral range (FSR). The FSR is given by:
$$\Delta x_{FSR} = \frac{\alpha}{M d_\omega} \tag{28}$$
This will set the grating order m through:
$$m = \frac{1}{2M} \frac{n_{s,TM}(\nu_0)}{n_{s,TE}(\nu_0)} \frac{n_{c,TE}(\nu_0)}{n_{c,TE}(\nu_0) - n_{c,TM}(\nu_0)} \tag{29}$$
Note that this maximizes spectral usage, as half of the spatial FSR is filled with TE, whereas the other half with TM channels/wavelengths. Following [13], the array order m is not the order of the demultiplexer, because the waveguide and material dispersion must be taken into account through the group index n_g. It can be incorporated through the modified grating order $m' = (n_g/n_{c,TE})\, m$.

3. Use Eq. (8) to obtain the necessary incremental length between arrayed waveguides Δl. The used $\Delta l'$ for each subarray will be M times the calculated Δl.

4. Calculate the loss nonuniformity L_u due to $B_g(x_3)$ in Eq. (18) through:
$$L_u(\mathrm{dB}) = 20\log_{10}\left(\frac{B_g(0)}{B_g(\Delta x_{Lu})}\right) \tag{30}$$
where the worst case is considered an output waveguide located a distance Δx_{Lu} that corresponds to M-1 grating orders shift of the central grating order m, and a central input waveguide. This will allow to place the input waveguides in any point in the input plane. Hence, the loss nonuniformity will be:
$$L_u(\mathrm{dB}) = 20\log_{10}\left(\frac{1}{e^{-\left(\pi\omega_g \frac{M-1}{M d_\omega}\right)^2}}\right) \tag{31}$$
From here it is possible to obtain the arrayed waveguides distance d_ω.

5. Obtain the frequency 3-dB bandwidth by using [9]:
$$\Delta\nu_{bw} = 2\gamma\omega_0\sqrt{2\ln\left(10^{3/20}\right)} \tag{32}$$
and derive the focal length L_f with Eqs. (20) and (3). Note that the FSDP parameter γ has to take into account the dispersion through the modified grating order m'.

6. Calculate the output waveguide distance through:

$$L_f = \nu_0 \frac{n_s}{n_g} \frac{d_0}{\Delta f_{ch}} \frac{d_\omega}{\Delta l} \tag{33}$$

where n_g is the group index of the arrayed waveguides [17].

7. Finally, the input waveguides will be positioned equidistant to the center of the input plane x_0 and separated a fraction M of the focussing zone. In the case of a 90° optical hybrid with 4 subarrays, the input waveguides will be at the positions $\pm\frac{1}{2}\alpha_{TE}(\nu_o)/(Md_\omega)$.

5. Simulation of a device using the design procedure

In Section 2, the validation of the model using fabricated devices parameters available in the literature was presented. Section 4 followed with the proposal of a novel design procedure, based on the proposed mode. In this section the procedure is used to design an IC-AWG from high level specifications. Besides, the design shown in this section provides a so-called universal design that can be used for groups of four wavelength channels at C-band, with 0.8 nm channel spacing. To be precise, the purpose of this device is to obtain a reusable structure that works not only in the four channels spaced 0.8 nm from 1550 nm to 1552.4 nm, but for other groups of four channels too.

1. The first choice for the design is the number of channels, set to 4 channels in this case, and the frequency/wavelength separation between them 100 GHz/0.8 nm.

2. Next, through Eq. (27), it is possible to calculate the cross-section related feature (PDWS) required for the arrayed waveguides. The simulated waveguides consist of a InGaAsP core with 160 nm of thickness with InP above and below, 1.9 μm of width, an etching of 0.2 μm and a cladding height of 1 μm. It is important to see that while the waveguide width is 1.9 μm, the gaussian width is 0.7 μm, obtained through curve fitting of the actual mode with commercial software [16]. The array waveguides effective indexes obtained for TE and TM polarizations are 3.1903 and 3.1826, respectively, and the slab couplers effective indexes for TE and TM are 3.2150 and 3.2048, respectively. Once the PDWS is fixed to 3.2 nm, the next step is to calculate the grating order to set it as a half FSR through Eq. (29), obtaining $m = 52$. The modified grating order is 60.72. Recall from Section 4 half of the FSR is filled with TE and the other half with TM channels/wavelengths.

3. Using this grating order the incremental length between arrayed waveguides Δl will be 25.264 μm, and incremental length in each subarray will be four times this increment.

4. The desired loss nonuniformity L_u is 1 dB, so using Eq. (31) is possible to obtain the arrayed waveguide distance $d_\omega = 4.861$ μm.

5. The frequency 3-dB bandwidth is fixed to 25 GHz, so the focal length L_f will be 1.5 mm through Eq. (32). The FSDP is calculated using $\gamma = (\nu_0 d_\omega)/(\alpha m')$.

6. By means of this focal length it is possible to obtain the distance between output waveguides $d_0 = 4.65$ μm using Eq. (33).

7. Finally, the input waveguides are placed at the positions 18.53 and -18.53 μm at the input plane x_0, respectively. Fig. 6 shows the resulting field at the output plane. It is possible to see that all the channels for both polarizations are placed almost equidistant.

Table 3: Summary of the IAWG design example parameters. Subscripts i, g and o stand for input, arrayed and output waveguides, respectively.

Technical Setup		Requirements		Physical parameters	
n_s	3.2150	N_o	32	N	120
n_c	3.1903	ν_o	193.1 THz	W_g	1.9 μm
W_i, W_g, W_o	1.9 μm	L_u	1 dB	W_i	1.9 μm
$\omega_i, \omega_g, \omega_o$	0.7 μm	$\Delta\nu_{bw}$	25 GHz	W_o	1.9 μm
Test Sheet				N_o	32
Requirement	Target	Obtained	Deviation (%)	d_i	37.06 μm
$\Delta\nu_c$	100 GHz	100 GHz	0	d_o	4.65 μm
$\Delta\lambda_{FSR}$	6.3819 nm	6.4 nm	0.28	m	52
L_d	1 dB	0.9736 dB	2.71	L_f	1.5 mm
$\Delta\nu_{bw}$	25 GHz	29.32 GHz	17.28	Δl	25.264 μm

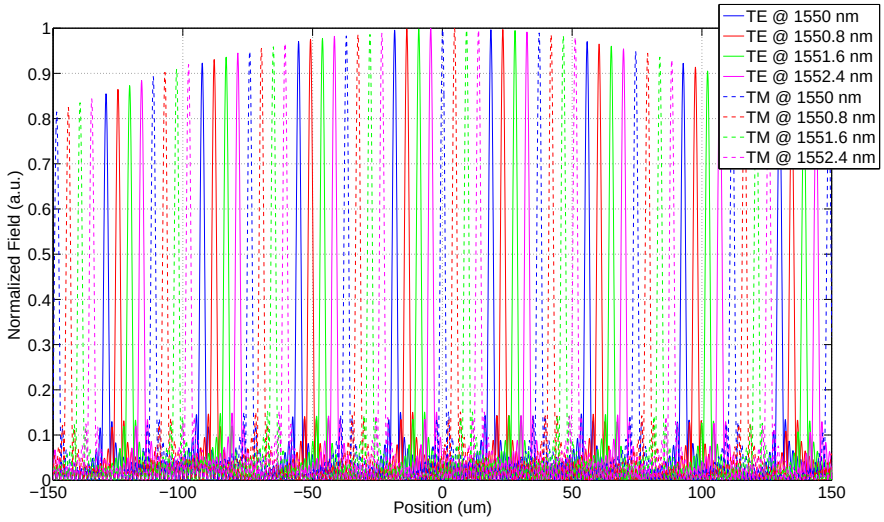

Fig. 6: Field at the output plane x_3 using input waveguide 1 for each channel and polarization

Moreover, the loss nonuniformity fixed to 1 dB is accomplished at the 32 output positions where output waveguides will be, as can be seen in Fig. 7 where there are represented the transfer function at the corresponding output waveguides of channel 1 for both polarizations. Table 3 shows a summary of the design parameters and the deviation about the target value.

6. Outlook and conclusion

The IC-AWG designed in Section 5 has two input waveguides and works in groups of 4 channels with a spacing of 0.8 nm. The design procedure sets the wavelength spacing between groups of 4 channels (FSR) to two times the PDWS, i.e. FSR = 6.4 nm. Accordingly, if the first group of 4 wavelength channels used for TE polarization are 1550.0, 1550.8, 1551.6 and 1552.4 nm, the next group of 4 channels with TE response in the same output waveguides starts at 1556.4 nm. Consequently, it may appear that the proposed design is not universal, as for TE polarization the 4 wavelengths 1553.2, 1554.0, 1554.8, 1555.6 nm, cannot be obtained from

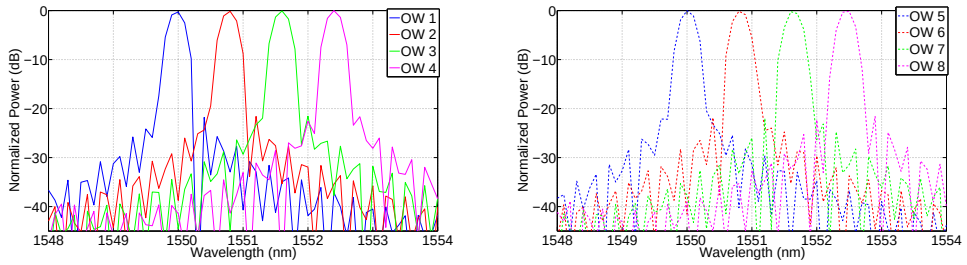

(a) (b)

Fig. 7: Transfer function at (a) output waveguides 1 to 4 at TE polarization and (b) output waveguides 5 to 8 at TM polarization

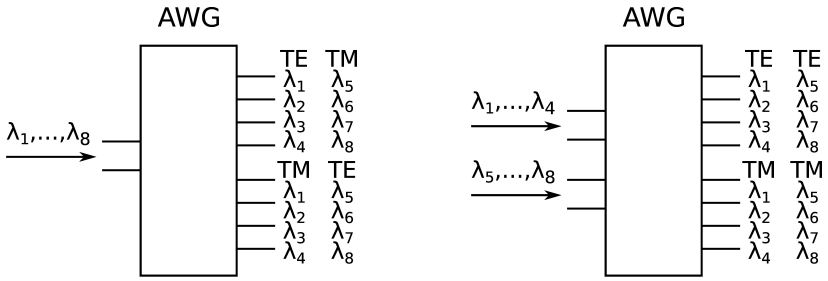

(a) IC-AWG with 2 input waveguides (b) IC-AWG with 4 input waveguides

Fig. 8: Schematic of IC-AWG with (a) two input waveguides, obtaining at the output waveguides response for each polarization in two channels per OW, and with (b) four input waveguides, obtaining at the output waveguides response in two channels but at the same polarization state.

the device. Nonetheless, there are two possible methods to obtain response in all the frequency band without spectral gaps (colorless) between the groups of channels for a given polarization.

The first method is shown in Fig. 8(a), where there are only two IW. As can be seen, the first four OW have response for the four first channels (1550, 1550.8, 1551.6 and 1552.4 nm, respectively) at TE polarization, and the second four OW have response at the same channels for TM polarization. If the same output waveguides are used with the next four channels (1553.2, 1554, 1554.8 and 1555.6 nm) at the input, then the first four OW have response for TM at this channels and the second four OW have response for TE polarization. Therefore, in the case only 4 input wavelengths are used, the wavelengths are demultiplexed by the IC-AWG, but the TE/TM ports are exchanged. Moreover, if 8 wavelengths are used in the device, it is still possible to use polarization splitters at the output waveguides, so polarization demultiplexing would follow each output of the IC-AWG.

The second method to obtain colorless operation is by means of two additional input waveguides, i.e. 4 input waveguides in total (Fig. 8(b)). As has been shown in Section 3, to obtain the 90° optical hybrid operation is necessary to put the two input waveguides with a spacing that is 1/4 of the BZ. Then, it is possible to obtain the response in the same OW for the same polarization state at the next group of four channels if the two new IWs are spaced 1/8 of the BZ with respect to the other two IWs. With this configuration, by spatially selecting the pair of inputs at the IC-AWG, demultiplexing and polarization splitting is performed, and no exchange be-

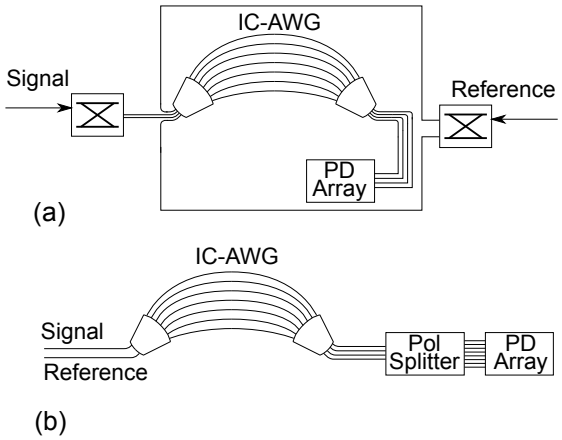

Fig. 9: (a) Schematic of a coherent detector using a four input waveguides IC-AWG with optical switches. (b) Schematic of a coherent detector using a two input waveguides IC-AWG with polarization splitter. Abbreviations: LO, local oscillator; PD array, photodetector array; Pol splitter, polarization splitter.

tween TE/TM ports happens (contrary to the previous case). The selection for the pair of input waveguides can happen at a packaging level, or at the chip level by means of integrated optical switches, as depicted in Fig. 9. An universal design may find applications, amongst other, in coherent optical integrated multi-wavelength receivers [8] and real-time optical arbitrary waveform measurement (OAWM) [18].

Possible drawbacks of this device are the larger number of output channels required compared to a regular AWG. For each input wavelength, the IC-AWG requires 8 output waveguides (two polarizations and four different phases). This can be limiting depending on the integration technology. AWGs have been reported with 32 outputs in InP [8] and with 40 outputs in SOI [19]. This number of output ports has to be divided by 8 to obtain the possible output channels in an IC-AWG. Also, there may be walk-off problems due to the large slab couplers when using it in a colorless application, but they might be overcome with design techniques similar to those reported in [20] for cyclic AWGs.

In conclusion, this paper provides a theoretical design and analysis model for an IC-AWG. The model is able to describe the operation as 90° hybrid, channel demultiplexing and polarization splitting. The model has been validated by means of parameters reported in the literature for fabricated coherent optical receivers. The model has been also used to develop a design procedure, which is a novel tool to obtain the most important physical parameters of the IC-AWG from targetted high level specifications. Finally, the design procedure and the accompanying discussions show how universal (colorless) devices can be designed and analyzed by means of the proposed model.

Acknowledgments

The authors acknowledge financial support by the Spanish MICINN Project TEC2010-21337, acronym ATOMIC; project FEDER UPVOV10-3E-492 and project FEDER UPVOV08-3E-008. B. Gargallo acknowledges financial support through FPI grant BES-2011-046100.